

# Testing and improving shear viscous phase space correction models

Mridula Damodaran and Denes Molnar

*Department of Physics and Astronomy, Purdue University, West Lafayette, IN 47907 and  
Wigner Research Center for Physics, Budapest, Hungary*

Gergely Gábor Barnaföldi, Dániel Berényi, and Máté Ferenc Nagy-Egri  
*Wigner Research Center for Physics, Budapest, Hungary*

(Dated: October 2, 2018)

Comparison of hydrodynamic calculations with experimental data inevitably requires a model for converting the fluid to particles. In this work, nonlinear  $2 \rightarrow 2$  kinetic theory is used to assess the overall accuracy of various shear viscous fluid-to-particle conversion models, such as the quadratic Grad corrections, the Strickland-Romatschke (SR) ansatz, self-consistent shear corrections from linearized kinetic theory, and the correction from the relaxation time approach. We test how well the conversion models can reconstruct, using solely the hydrodynamic fields computed from the transport, the phase space density for a massless one-component gas undergoing a 0+1D longitudinal boost-invariant expansion with approximately constant specific shear viscosity in the range  $0.03 \lesssim \eta/s \lesssim 0.2$ .

In general we find that at early times the SR form is the most accurate, whereas at late times or for small  $\eta/s \sim 0.05$  the self-consistent corrections from kinetic theory perform the best. In addition, we show that the reconstruction accuracy of additive shear viscous  $f = f_{eq} + \delta f$  models dramatically improves if one ensures, through “exponentiation”, that  $f$  is always positive. We also illustrate how even more accurate viscous  $\delta f$  models can be constructed if one includes information about the past evolution of the system via the first time derivative of hydrodynamic fields. Such time derivatives are readily available in hydrodynamic simulations, though usually not included in the output.

## I. INTRODUCTION

Relativistic viscous hydrodynamics is probably the most popular framework to model ultrarelativistic heavy-ion collisions (for reviews, see, e.g., Refs. [1–3]). Its strong appeal is that it describes the evolution directly utilizing bulk matter properties such as the equation of state and the shear and bulk viscosities. However, at least for heavy-ion physics applications, the framework is incomplete. First, the early evolution is far from local thermal equilibrium; therefore, a model of initial conditions is needed. Second, comparison with experimental data inevitably requires a model for converting the fluid to particles. This so-called “particlization” [4–6], which is our focus here, is necessary irrespectively of whether one compares hydrodynamics directly with experiments, or combines hydrodynamics with subsequent hadronic transport (“hybrid” approach) [7–9].

For fluids in perfect local equilibrium, i.e., *ideal* fluids, the conversion to particles is straightforward, at least as long as one models the fluid, at the conversion point, as an ideal gas of hadrons. Then, the phase space densities of the various hadron species are uniquely determined by the hydrodynamic fields. In contrast, *viscous* fluids are in general out of local equilibrium, which makes the conversion ambiguous because an infinite class of phase space densities reproduces the same hydrodynamic fields[5] (this is so even for a one-component gas). Several different particlization models are in use based on Grad’s quadratic form[10, 11], the Romatschke-Strickland ansatz[12, 13], the linearized Boltzmann transport equation[5, 14, 15], or kinetic theory in the relaxation time approach[14, 16]; all of which originate from kinetic theory.

It is not clear *a priori* which particlization schemes, if any, are accurate. In this paper we investigate how well different approaches can reproduce *shear* corrections generated by fully nonlinear  $2 \rightarrow 2$  transport theory. The study here shares similarities with an earlier work [17] by one of us, in which transport solutions obtained with Molnar’s Parton Cascade (MPC) [18] for a one-component gas in a 0+1D Bjorken scenario were used to test formulations of viscous hydrodynamics. However, instead of studying how well hydrodynamic models follow the evolution of the energy-momentum tensor in the transport, here we investigate how well particlization models reproduce the actual phase space distribution in the transport from the exact hydrodynamic fields corresponding to the transport solution.

In addition, we present two improvements to current shear viscous  $\delta f$  models. First, we cure the unphysical negative contributions in additive  $f = f_{eq} + \delta f$  models, and show that this leads to a dramatic improvement in accuracy. Moreover, we illustrate how knowledge of the first time derivative of hydrodynamic fields, which is readily available in hydrodynamic calculations, can be used to intelligently switch between viscous correction models to apply them closer to their respective regions of validity.

The structure of the paper is as follows. A brief introduction to the general problem in Sec. II is followed by a

discussion of four different shear viscous  $\delta f$  models in Sec. III. Next, Sec. IV outlines covariant transport theory and the MPC/Grid numerical transport solver, and Sec. V describes how the  $\delta f$  models are tested against kinetic theory. Finally, Sec. VI presents the results on the overall accuracy of the four shear viscous  $\delta f$  models, as well as, novel improvements to current  $\delta f$  models.

## II. AMBIGUITY IN CHOOSING VISCOUS PHASE SPACE CORRECTIONS

We briefly review here the challenge posed by the ambiguity in constructing phase space distributions from hydrodynamics. Only the case of a one-component system will be discussed (see, e.g., Ref. [5] for multi-component mixtures). For a noninteracting gas, the hydrodynamic fields, namely, the energy-momentum tensor and the number current[28] are directly given by the (on-shell) phase space density  $f \equiv dN/d^3x d^3p$  as

$$T^{\mu\nu}(x) \equiv \int \frac{d^3p}{E} p^\mu p^\nu f(x, \mathbf{p}) , \quad N^\mu(x) \equiv \int \frac{d^3p}{E} p^\mu f(x, \mathbf{p}) . \quad (1)$$

In local equilibrium[29]

$$f^{\text{eq}}(x, \mathbf{p}) = \frac{g}{(2\pi)^3} \exp \left[ \frac{\mu(x) - p^\alpha u_\alpha(x)}{T(x)} \right] , \quad (2)$$

which reproduces the fields in ideal (nonviscous) hydrodynamics:

$$T_{\text{eq}}^{\mu\nu} = (e + p)u^\mu u^\nu - p g^{\mu\nu} , \quad N_{\text{eq}}^\mu = n u^\mu . \quad (3)$$

Here,  $g$  is the number of internal degrees of freedom,  $e$ ,  $p$ ,  $n$ ,  $u$ ,  $T$ , and  $\mu$  are the local energy density, equilibrium pressure, particle density, flow velocity, temperature, and chemical potential, respectively, and we dropped the space-time argument  $x$  for brevity. For ideal fluids the phase space density is uniquely determined by the hydrodynamic fields because straightforward inversion of (3) gives

$$n = \sqrt{N_{\text{eq}}^\mu N_{\text{eq},\mu}} , \quad u^\mu = \frac{N_{\text{eq}}^\mu}{n} , \quad e = u_\mu T_{\text{eq}}^{\mu\nu} u_\nu , \quad (4)$$

and through the equations of state  $p(e, n)$ ,  $T(e, n)$ , and  $\mu(e, n)$  these give the local temperature and chemical potential. Specifically, for the massless Boltzmann particles considered later here,

$$p = \frac{e}{3} , \quad T = \frac{p}{n} = \frac{e}{3n} , \quad \mu = T \ln \frac{n}{n_{\text{eq}}(T)} = T \ln \frac{27\pi^2 n^4}{g e^3} \quad (5)$$

( $n_{\text{eq}} = gT^3/\pi^2$  is the thermal particle density at  $\mu = 0$ , i.e., in local thermal *and* chemical equilibrium).

In the general out-of-local-equilibrium case, one can split the phase space density into a local equilibrium piece and a dissipative correction as  $f(x, \mathbf{p}) \equiv f_{\text{eq}}(x, \mathbf{p}) + \delta f(x, \mathbf{p})$  [30]. Consequently, nonequilibrium corrections arise to the hydrodynamic fields as well:

$$\delta T^{\mu\nu}(x) = \int \frac{d^3p}{E} p^\mu p^\nu \delta f(x, \mathbf{p}) , \quad \delta N^\mu(x) = \int \frac{d^3p}{E} p^\mu \delta f(x, \mathbf{p}) . \quad (6)$$

Here  $\delta T^{\mu\nu}$  contains shear stress and bulk pressure corrections, whereas  $\delta N^\mu$  describes particle diffusion. While dissipative hydrodynamics solutions provide both the ideal part and the dissipative corrections to all hydrodynamic fields, phase space densities are not available from hydrodynamics because the correction  $\delta f$  is not known. The challenge to particlization models is to invert (6) for  $\delta f$ . Inversion is only possible with additional theory input because an infinite class of different phase space distributions reproduces the same hydrodynamic fields[19].

## III. MODELS FOR SHEAR VISCOUS PHASE SPACE CORRECTIONS

From here on we focus on phase space corrections due to shear only, i.e., we take

$$\delta T^{\mu\nu}(x) = \pi^{\mu\nu}(x) , \quad \delta N^\mu(x) = 0 , \quad (7)$$

where  $\pi^{\mu\nu}(x)$  is the local shear stress. It is a symmetric, traceless tensor that is purely spatial in the local rest (LR) frame of the fluid:

$$u_\mu \pi^{\mu\nu} = 0 = \pi^{\nu\mu} u_\mu , \quad \pi^\mu_\mu = 0 . \quad (8)$$

(In the LR frame,  $u_{LR}^\mu = (1, \mathbf{0})$ .) Below we review popular parametrizations for shear viscous phase space corrections.

### A. Grad ansatz

A natural starting point for near-equilibrium phase space distributions is an expansion in small gradients around local equilibrium [5, 10, 11, 17] (also, Ch. VII of [20]):

$$f(x, \mathbf{p}) = f_{eq}(x, \mathbf{p}) [1 + \phi(x, \mathbf{p})] \quad \text{with} \quad |\phi| \ll 1, \quad |p^\mu \partial_\mu \phi| \ll |p^\mu \partial_\mu f_{eq}| / f_{eq}. \quad (9)$$

The commonly used Grad ansatz then comes from a Taylor expansion of  $\phi$  in powers of the momentum:

$$\phi(x, \mathbf{p}) = D^\mu(x) p_\mu + C^{\mu\nu}(x) p_\mu p_\nu + \mathcal{O}(p^3). \quad (10)$$

If there is no particle diffusion and no bulk pressure either[31], then  $D^\mu = 0$ , which leads to

$$\phi_{Grad}(x, \mathbf{p}) = \frac{\pi^{\mu\nu}}{2(e+p)} \frac{p_\mu p_\nu}{T^2} = \frac{\pi^{\mu\nu}}{8p} \frac{p_\mu p_\nu}{T^2}, \quad (11)$$

where in the last step we specialized to a gas of massless particles ( $e = 3p$ ). The  $p_\mu p_\nu \pi^{\mu\nu}$  term introduces a characteristic quadratic momentum dependence. The Grad ansatz also played a key role in the Israel-Stewart formulation of causal relativistic viscous hydrodynamics [11].

### B. Strickland-Romatschke form (SR)

Another class of nonthermal phase space distributions has been proposed based on stretching a spherically symmetric momentum distribution [12]:

$$f(|\mathbf{p}|) \rightarrow f\left(\sqrt{p_T^2 + a^2 p_z^2}\right), \quad p_T \equiv \sqrt{p_x^2 + p_y^2}. \quad (12)$$

This form was originally motivated as a convenient way to introduce transverse vs longitudinal momentum anisotropy via a single parameter  $a$ . For transversely homogeneous, longitudinally boost invariant dynamics with massless particles, the Strickland-Romatschke (SR) ansatz reads

$$f_{SR}(x, \mathbf{p}) \equiv f_{eq} + \delta f_{SR} = N \exp\left(-\frac{1}{\Lambda} \sqrt{p_{LR,T}^2 + a^2 p_{LR,z}^2}\right). \quad (13)$$

The advantage of the SR ansatz is that it is strictly positive everywhere, and for  $a = 0$  it describes local thermal equilibrium, while for  $a = \tau/\tau_0$  it gives back the free streaming evolution for massless particles as long as the system started at  $\tau = \tau_0$  from local thermal equilibrium. Here  $\tau$  is the Bjorken proper time (cf. Sec. V A).

More complicated anisotropies can be accommodated via suitable generalizations of the ansatz [13, 21]. The SR ansatz and its extensions are also employed in the formulation of anisotropic hydrodynamics[22].

### C. Self-consistent viscous corrections from linearized covariant transport

In contrast to ad-hoc parametrizations, self-consistent viscous corrections can be obtained from relativistic kinetic theory[5]. These follow from the relativistic Boltzmann transport equation (BTE), if one linearizes in the departure from local equilibrium, and studies the late-time asymptotic evolution in the presence of flow gradients in the system. We refer the Reader to Refs. [5, 14, 15] for details of the procedure. For shear, one can show that

$$\delta f_{lin} = \chi\left(\frac{\mathbf{p} \cdot \mathbf{u}}{T}\right) \frac{p_\mu p_\nu \sigma^{\mu\nu}}{T^3} f_{eq}, \quad (14)$$

where the dimensionless function  $\chi$  is the solution to a linear integral equation

$$p^\mu \nabla_\mu f_{eq} = L[\delta f_{lin}], \quad (15)$$

and the shear tensor

$$\sigma^{\mu\nu} \equiv \nabla^\mu u^\nu + \nabla^\nu u^\mu - \frac{2}{3} \Delta^{\mu\nu} (\partial \cdot u) \quad (16)$$

characterizes shear deformation of the flow field. The projector  $\Delta^{\mu\nu} \equiv g^{\mu\nu} - u^\mu u^\nu$  and the gradient  $\nabla^\mu \equiv \Delta^{\mu\nu} \partial_\nu$  orthogonal to the flow ensure that  $\sigma^{\mu\nu}$  is traceless and in the LR frame purely spatial.

In general, the integral equation must be solved for  $\chi$  numerically. Replacing the shear tensor with the shear stress tensor using the Navier-Stokes relation  $\pi^{\mu\nu} = \eta \sigma^{\mu\nu}$  gives

$$\delta f_{lin} = \chi \left( \frac{p \cdot u}{T} \right) \frac{p_\mu p_\nu \pi^{\mu\nu}}{\eta T^3} f_{eq} , \quad (17)$$

which is the same as the quadratic Grad form but generalized to a self-consistently determined function of momentum. For isotropic  $2 \rightarrow 2$  scattering with constant cross sections, the self-consistent viscous corrections are well approximated[5] by  $\chi(x) \approx const/\sqrt{x}$ , i.e.,  $\delta f/f_{eq}$  has  $\sim p^{3/2}$  momentum dependence. Interestingly, the same  $3/2$  exponent arises from kinetic theory with forward-peaked  $1 \leftrightarrow 2$  perturbative QCD matrix elements[14].

#### D. Relaxation time approximation (RTA)

Alternatively, one might treat the Boltzmann transport equation in the relaxation time approximation[14, 16] (RTA):

$$p^\mu \partial_\mu f(x, \mathbf{p}) = -\frac{p \cdot u}{\tau_{eq}} (f(x, \mathbf{p}) - f_{eq}(x, \mathbf{p})) . \quad (18)$$

At late times, the system relaxes to equilibrium and  $\partial_t f \rightarrow 0$ . In this regime, one can perform a calculation analogous to that for the self-consistent viscous corrections of Sec. III C but with the simplified RTA kernel. For the RTA, (15) reads

$$p^\mu \nabla_\mu f_{eq} = -\frac{p \cdot u}{\tau_{eq}} \delta f_{RTA} . \quad (19)$$

For pure shear deformation of the flow fields[5],

$$p^\mu \nabla_\mu f_{eq} = -\frac{1}{2T} p_\mu p_\nu \sigma^{\mu\nu} f_{eq} , \quad (20)$$

which then leads to

$$\delta f_{RTA} = \frac{\tau_{rel}}{2T(p \cdot u)} \sigma^{\mu\nu} p_\mu p_\nu f_{eq} . \quad (21)$$

Thus, if the relaxation time does not depend on momentum, then the shear correction from the RTA is linear in momentum for massless particles. (Other powers could be accommodated with appropriate momentum dependent  $\tau_{rel}$  [14].)

#### E. Power law generalization of Grad ansatz (PG)

A simple generalization of the Grad shear correction (11) is to include arbitrary  $p^\alpha$  power ( $\alpha > 0$ ) of the momentum via

$$\phi_{PG}(x, \mathbf{p}) = C(\alpha) \left( \frac{p \cdot u}{T} \right)^{\alpha-2} \frac{\pi^{\mu\nu} p_\mu p_\nu}{8p T^2} , \quad C(\alpha) = \frac{5!}{(3+\alpha)!} . \quad (22)$$

The coefficient  $C(\alpha)$  is set by the requirement that  $\phi$  gives back the correct shear stress through (6), and we have used that the particles are massless (this form was also discussed in [14]).

Setting  $\alpha = 2$  gives back the quadratic Grad ansatz of Sec. III A. On the other hand, as we saw in Sec. III C, shear viscous  $\delta f$  calculations based on linearized kinetic theory are well approximated by a significantly smaller  $\alpha \approx 3/2$ . Shear viscous corrections based on the relaxation time approximation (Sec. III D) correspond to a yet smaller  $\alpha = 1$  exponent (if the relaxation time is constant). Thus, the power-law Grad form can conveniently capture three rather different models. *In what follows we are going to concentrate on four different shear viscous  $\delta f$  models: the power-law Grad ansatz with exponents  $\alpha = 1$  (RTA),  $3/2$  (full BTE), and  $2$  (Grad), and the Strickland-Romatschke form.*

A shortcoming of both the Grad ansatz and its power law extension is that at high momenta the phase space distribution  $f$  can become negative. The shear stress tensor is traceless, so it has positive and negative eigenvalues. Therefore,  $p_\mu p_\nu \pi^{\mu\nu}$  is not bounded from below. A possible remedy through ‘‘exponentiation’’ is discussed in Sec. V C.

## IV. COVARIANT TRANSPORT THEORY

Let us now turn to discussing covariant transport theory that will be used to test the accuracy of shear viscous  $\delta f$  models.

### A. Boltzmann transport equation

Consider on-shell covariant transport theory for a system with  $2 \rightarrow 2$  interactions as, e.g., in Refs. [17, 23] (for a discussion of the multicomponent case, see [5]). The evolution of the phase space density is given by the nonlinear Boltzmann transport equation

$$p^\mu \partial_\mu f(x, \mathbf{p}) = S(x, \mathbf{p}) + C[f](x, \mathbf{p}) , \quad (23)$$

where the source term  $S$  encodes the initial conditions, and the two-body collision term is

$$C[f](x, \mathbf{p}_1) \equiv \iiint_{234} (f_3 f_4 - f_1 f_2) \bar{W}_{12 \rightarrow 34} \delta^4(12 - 34) \quad (24)$$

with shorthands  $\int \equiv \int d^3 p_a / (2E_a)$ ,  $f_a \equiv f(x, \mathbf{p}_a)$ , and  $\delta^4(ab - cd) \equiv \delta^4(p_a + p_b - p_c - p_d)$ . The transition probability  $\bar{W}_{12 \rightarrow 34}$  for  $2 \rightarrow 2$  scattering with momenta  $p_1 + p_2 \rightarrow p_3 + p_4$  is given by the differential cross section as  $\bar{W} = 4s d\sigma / d\Omega_{cm}$ , where  $s \equiv (p_1 + p_2)^2$  is the usual Mandelstam variable, and the solid angle is taken in the c.m. frame of the microscopic two-body collision.

### B. Numerical solutions via the MPC/Grid algorithm

To compute transport solutions numerically, we utilize a new parallelized version of the MPC/Grid solver from Molnar's Parton Cascade (MPC) [18]. Details of the algorithm will be published elsewhere, so here we only focus on the key ingredients. Similarly to the Boltzmann Approach to Multi-Parton Scattering code (BAMPS) [24], MPC/Grid uses test particles on a three-dimensional spatial grid, which undergo random scatterings. Between scatterings, the test particles move on straight lines. In each time step  $\Delta t$ , in each cell, pairs of test particles are tested for  $2 \rightarrow 2$  scattering with probability  $P_{2 \rightarrow 2} = \sigma v_{rel} \Delta t / V_{cell}$ , where  $\sigma$  is the total cross section,  $v_{rel} \equiv \sqrt{(p_1 \cdot p_2) - m_1^2 m_2^2} / E_1 E_2$  is the relative velocity of the pair, and  $V_{cell}$  is the volume of the cell. If a scattering occurs, outgoing momenta are generated according to the differential cross section. MPC/Grid can also take  $2 \leftrightarrow 3$  scatterings into account but those were not turned on in this study.

Formally, the grid algorithm obtains the correct transport solution in the limit of small time steps, small cell sizes, and large number of test particles. This gives extra flexibility compared to cascade algorithms based on scattering at closest approach. In the cascade approach, numerical artifacts can only be reduced via increasing the number of test particles through particle subdivision [23, 25]  $N_{test} \rightarrow \ell N_{test}$ . Therefore, in the cascade, the effective range of nonlocal interactions decreases as  $1/\sqrt{\ell}$  jointly in all three principle directions. In contrast, the grid approach controls the effective range of nonlocality independently in each principle direction through the cell sizes in those directions, which enables much faster calculations in situations with high symmetry. For example, in the 0+1D (transversely homogeneous and static) Bjorken scenario of Sec. V, the cell size only needs to be small in the rapidity  $\eta$  direction, but in the transverse directions it can stay arbitrarily large. Reduction of the effective range by a factor  $\lambda$  requires  $\mathcal{O}(\lambda^4)$  times longer computation with the cascade method, but not worse than  $\mathcal{O}(\lambda^3)$  with the grid approach (in fact, only  $\mathcal{O}(\lambda)$  if  $N_{test}$  is sufficiently large).

## V. TESTING $\delta f$ MODELS

Let us turn to the specifics of the transport calculations and comparisons used to gauge the accuracy of viscous  $\delta f$  models.

### A. Calculation setup

To study the accuracy of shear viscous  $\delta f$  models, we consider a system of massless particles evolving in a 0+1D Bjorken scenario. Transversely, the system is static, homogeneous, and rotation invariant (in the actual calculation, periodic boundary conditions are imposed). Longitudinally, the system undergoes boost-invariant[32] Bjorken expansion, and we also impose  $z \rightarrow -z$  reflection symmetry. This scenario has been extensively studied, e.g., in [17], so we only remind the Reader of a few important features here.

A convenient set of coordinates is provided by the Bjorken proper time  $\tau$ , coordinate rapidity  $\eta$ , momentum rapidity  $y$ , and transverse momentum  $p_T$ , defined via

$$\tau \equiv \sqrt{t^2 - z^2}, \quad \eta \equiv \frac{1}{2} \ln \frac{t+z}{t-z}, \quad y \equiv \frac{1}{2} \ln \frac{E+p_z}{E-p_z}, \quad p_T \equiv \sqrt{p_x^2 + p_y^2}. \quad (25)$$

Due to the high degree of symmetry, the phase space density only depends on  $p_T$ ,  $\xi \equiv \eta - y$ , and  $\tau$ . Since  $f(p_T, \xi, \tau) = f(p_T, -\xi, \tau)$ , it is often convenient to consider that the  $\xi$  dependence is through  $\text{ch} \xi$ . The local flow velocity and particle density of the system are

$$u^\mu = (\text{ch} \eta, \mathbf{0}_T, \text{sh} \eta), \quad n(\tau) = \frac{\tau_0}{\tau} n_0, \quad (26)$$

where  $n_0 \equiv n(\tau_0)$  and

$$n(\tau) = 4\pi \int_0^\infty dp_T p_T^2 \int_0^\infty d\xi \text{ch} \xi f(\xi, p_T, \tau). \quad (27)$$

The energy momentum tensor is diagonal in the LR frame, and because bulk viscosity and the bulk viscous pressure vanish for massless particles, it reads

$$T_{LR}^{\mu\nu} = T^{\mu\nu}(\eta = 0) = \text{diag}\left(e, p - \frac{\pi_L}{2}, p - \frac{\pi_L}{2}, p + \pi_L\right) \quad \text{with} \quad p = \frac{e}{3}. \quad (28)$$

There are only two remaining independent hydrodynamic variables, the local comoving energy density and longitudinal shear stress, which are given by

$$e(\tau) = \int \frac{d^3 p}{E} (p \cdot u)^2 f = 4\pi \int_0^\infty dp_T p_T^3 \int_0^\infty d\xi \text{ch}^2 \xi f(p_T, \xi, \tau), \quad (29)$$

$$\pi_L(\tau) \equiv T_{LR}^{zz} - p = \int \frac{d^3 p}{E} \left( p_{z,LR}^2 - \frac{p_{LR}^2}{3} \right) f = 4\pi \int_0^\infty dp_T p_T^3 \int_0^\infty d\xi \left( \text{sh}^2 \xi - \frac{\text{ch}^2 \xi}{3} \right) f(p_T, \xi, \tau). \quad (30)$$

It will be more convenient later to use equivalent expressions in terms of the momentum distribution of particles[33]

$$F(p_T, \xi, \tau) \equiv \frac{dN}{dp_T d\xi d\eta} = 2\pi A_T \tau p_T^2 \text{ch} \xi f(p_T, \xi, \tau), \quad (31)$$

where  $A_T$  is the transverse area of the system. Then,

$$e(\tau) = \frac{2}{A_T \tau} \int_0^\infty dp_T p_T \int_0^\infty d\xi \text{ch} \xi F(p_T, \xi, \tau), \quad (32)$$

$$\pi_L(\tau) = \frac{2}{A_T \tau} \int_0^\infty dp_T p_T \int_0^\infty d\xi \left( \frac{\text{sh}^2 \xi}{\text{ch} \xi} - \frac{\text{ch} \xi}{3} \right) F(p_T, \xi, \tau), \quad (33)$$

$$n(\tau) = \frac{2}{A_T \tau} \int_0^\infty dp_T \int_0^\infty d\xi F(p_T, \xi, \tau). \quad (34)$$

Due to longitudinal boost invariance,  $F$  has no separate  $\eta$  dependence (it only depends on  $\eta$  through  $\xi$ ).

To mimic  $\eta/s \approx \text{const}$  dynamics[17], isotropic  $2 \rightarrow 2$  cross sections are used that grow with proper time as  $\sigma(\tau) = (\tau/\tau_0)^{2/3} \sigma_0$ . We start the system at  $\tau = \tau_0$  from local thermal equilibrium. If one uses dimensionless proper time  $\tau/\tau_0$  and dimensionless momenta  $p_T/T_0$ , then for massless particles the transport evolution depends only[23] on the initial inverse Knudsen number

$$K_0 \equiv \frac{\tau_0}{\lambda_{MFP}(\tau_0)} = n_0 \sigma_0 \tau_0, \quad (35)$$

which is the ratio of time scales for expansion and scattering. The inverse Knudsen number is tightly related[17] to the specific shear viscosity  $\eta/s$ , which is the dimensionless ratio of the shear viscosity and the entropy density. Replacing  $\sigma$  and  $n$  with the shear viscosity  $\eta \approx 1.2676T/\sigma$  and entropy density[34]  $s \sim 4n$  one obtains

$$K_0 \approx \frac{T_0 \tau_0 s}{5 \eta} . \quad (36)$$

For A+A reactions at top Relativistic Heavy Ion Collider (RHIC) and Large Hadron Collider (LHC) energies,  $T_0 \tau_0 \sim 1$  at particlization, so  $\eta/s \sim 1/(5K_0)$ . In what follows we will often refer to calculations by their approximate  $\eta/s$  value because that is of high interest within the community.

The transport evolution was computed for initial inverse Knudsen numbers in the range  $1 \leq K_0 \leq 6.47$  ( $0.03 \lesssim \eta/s \lesssim 0.2$ ). For each  $K_0$  value, high-statistics transport solutions corresponding to total 270 million test particles were calculated on the community clusters at the Rosen Center for Advanced Computing (RCAC) at Purdue. To ensure approximately boost-invariant evolution, the systems were initialized with uniform coordinate rapidity distribution  $dN/d\eta$  in a large initial coordinate rapidity window  $|\eta| < 6$ . Near the longitudinal  $\eta \sim \pm 6$  edges, boost invariance certainly does not apply. Therefore, only test particles close to midrapidity with  $|\eta| < y_0$  are analyzed. Boost invariance was monitored during the evolution through tracking  $dN/d\eta$  vs  $\eta$  and  $\tau$ . To ensure that relative  $dN/d\eta$  variations stay in all cases below 0.3% in the midrapidity window, we set  $y_0 = 2$ , which leaves about 90 million test particles for analysis at each value of  $K_0$ .

It is well known[17] that for  $\eta/s \approx \text{const}$ , the rapid longitudinal Bjorken expansion first drives the system away from local equilibrium but later the system relaxes back to local equilibrium. A convenient dimensionless parameter that measures the degree of departure from local equilibrium is the shear stress to pressure ratio

$$R_\pi \equiv \frac{\pi_L}{p} \quad (37)$$

(in local equilibrium  $R_\pi = 0$ ). As shown in Fig. 1, during early times  $\pi_L$  (and thus  $R_\pi$ ) becomes more and more negative but at late times  $\pi_L$  vanishes asymptotically. The larger  $K_0$  is, the closer the system stays to local thermal equilibrium. For  $\eta/s \approx 0.2$  ( $K_0 = 1$ ) shear stress becomes fairly large in magnitude, reaching  $|\pi_L| \approx 0.4p$ .

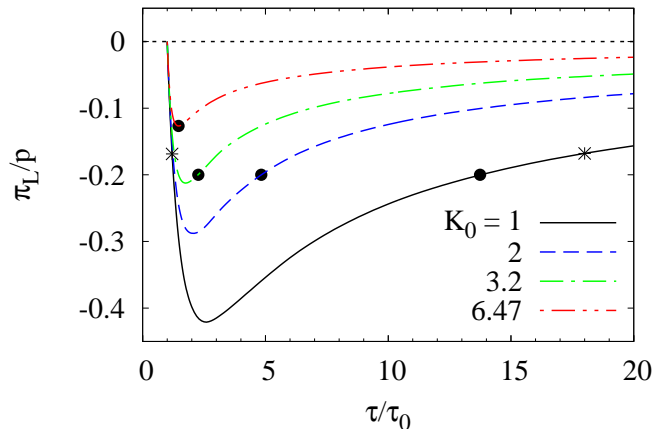


FIG. 1: Shear stress to equilibrium pressure ratio as a function of rescaled proper time  $\tau/\tau_0$  calculated with MPC/Grid for a massless system in a 0+1D Bjorken scenario with energy-independent, isotropic  $2 \rightarrow 2$  cross section. To mimic  $\eta/s \approx \text{const}$  evolution, the cross section was increasing with time proportionally to  $\tau^{2/3}$ . Results for initial Knudsen numbers  $K_0 = 1$  ( $\eta/s \sim 0.2$ , solid black), 2 ( $\eta/s \sim 0.1$ , dashed blue), 3.2 ( $\eta/s \sim 0.06$ , dashed-dotted green), and 6.47 ( $\eta/s \sim 0.03$ , dashed-double-dotted red line) are shown. Stars indicate the two time slices that are compared in Fig. 4, while filled circles show the switching times for the simple improved  $\delta f$  model in Fig. 5.

## B. Fitting $\delta f$ model parameters

The primary output of the transport code is the momentum distribution (31) of test particles crossing  $\tau = \text{const}$  hypersurfaces, given in terms of a list of test particles:

$$F_{tr}(p_T, \xi, \tau) = \frac{1}{2y_0\ell} \sum_{i=1}^{N_{test}} \delta(p_{T,i} - p_T) \delta(\xi_i - \xi) . \quad (38)$$

It is straightforward to apply (32), (33), and (34) to calculate the comoving energy density, longitudinal shear stress, and number density corresponding to the transport simulations (1/ $\sqrt{N}$  relative fluctuations in these quantities are about 0.1% with our statistics). Each simulation was then followed for each of the four  $\delta f$  models by an *inversion* of (29) (30), and (27) to match model parameters to the hydrodynamic fields at several proper times in the range  $1 \leq \tau/\tau_0 \leq 20$  chosen for analysis.

In Bjorken coordinates, the power-law Grad form and the Strickland-Romatschke ansatz read

$$f_{PG} = N \left[ 1 + \frac{15R_\pi}{(3+\alpha)!} \left( \frac{p_T}{T} \right)^\alpha \text{ch}^{\alpha-2}\xi \left( \text{sh}^2\xi - \frac{1}{2} \right) \right] e^{-p_T \text{ch}\xi/T} , \quad (39)$$

$$f_{SR} = N \exp\left( -\frac{p_T}{\Lambda} \sqrt{1 + a^2 \text{sh}^2\xi} \right) . \quad (40)$$

Thus, all  $\delta f$  models considered here have three parameters: an overall normalization factor  $N$ , a momentum scale ( $T$  or  $\Lambda$ ), and a dimensionless pressure anisotropy parameter ( $R_\pi$  or  $a$ ). It is, therefore, convenient to first match the anisotropy parameter to reproduce  $\pi_L/e$ , then set the momentum scale from the effective temperature

$$T_{eff} \equiv \frac{e}{3n} , \quad (41)$$

and finally get the normalization from  $n$ . This way, each step can be accomplished with root finding in only one dimension[35]. The necessary  $p_T$  and  $\xi$  integrals were performed numerically.

## C. Quantifying model accuracy

Our primary goal is to assess the accuracy of the four  $\delta f$  models of Sec. III, namely, how well they reconstruct the phase space density  $f$ , or equivalently, the momentum distribution  $F$ . The most differential comparison would be to study the relative reconstruction error in the  $p_T - \xi$  plane as a function of the proper time  $\tau$ , given by the ratio of the reconstructed distribution  $F_{rec}$  to the actual distribution  $F_{tr}$  from the transport as

$$\varepsilon(p_T, \xi, \tau) \equiv \frac{F_{rec}(p_T, \xi, \tau)}{F_{tr}(p_T, \xi, \tau)} - 1 . \quad (42)$$

It is more useful to take  $F_{rec}/F_{tr}$  and not  $F_{tr}/F_{rec}$  because that avoids poles if  $F_{rec}$  goes negative. Numerically, the transport distribution is represented by test particles, therefore it is more meaningful to compare two-dimensional histograms (integrated counts over small  $\Delta p_T \times \Delta \xi$  regions):

$$\varepsilon_{ij}(\tau) \equiv \frac{\int_{p_{T,i-1}}^{p_{T,i}} dp_T \int_{\xi_{j-1}}^{\xi_j} d\xi F_{rec}(p_T, \xi, \tau)}{\Delta N_{tr}(p_{T,i-1} \leq p_T < p_{T,i}, \xi_{j-1} \leq \xi < \xi_j)} - 1 , \quad p_{T,i} \equiv i\Delta p_T , \quad \xi_j \equiv j\Delta \xi \quad (i = 1, \dots, j = 1, \dots) . \quad (43)$$

However, this still gives too much information to present in a journal article.

Therefore, we compare here the root-mean-squared (RMS) relative error across all  $p_T - \xi$  bins for the various  $\delta f$  models as a function of  $\tau$ :

$$\varepsilon_{RMS}(\tau) \equiv \sqrt{\frac{1}{N_{bins}} \sum_{ij} \varepsilon_{ij}^2(\tau)} , \quad (44)$$

which characterizes the overall accuracy in terms of a single number. This is, purposefully, quite different from the popular  $\chi^2$  quantity used in data versus model comparisons because the terms in (44) are not divided by a statistical error estimate for the measured counts. In our case, all reconstruction models are only approximate (strictly speaking,

incorrect), and we want to determine their overall error in  $p_T$ - $\xi$  space. Therefore, as long as all counts in the histogram are measured with reasonable accuracy, there is no inherent value in giving larger weight to bins with very accurate counts. With  $\chi^2$  statistics, one would find for each model that  $\chi^2$  grows with the size of the statistical sample, indicating that statistically the models are less and less likely to be correct. In contrast, the root-mean-squared error converges with increasing sample size.

We evaluate  $\varepsilon_{ij}$  within bins of size  $\Delta p_T = 0.16T_0$  and  $\Delta\xi \approx 0.1$ , across the rectangular region  $p_T \leq 12T_{eff}$ ,  $|\xi| \leq 4$ . To limit statistical fluctuations, only bins with at least 200 counts are included in the average. The two-dimensional integrals needed in (43) were calculated via nesting one-dimensional adaptive Gauss-Kronrod quadrature routines from the GNU Scientific Library (GSL) [27], and using an OpenCL implementation of two-dimensional Simpson quadrature on graphics processor units (GPUs) at the GPU Laboratory of the Wigner Research Center for Physics (Budapest, Hungary).

## VI. RESULTS AND IMPROVED $\delta f$ MODELS

In this section we quantify the accuracy of the four shear viscous  $\delta f$  models discussed in Sec. III, and also discuss novel improvements to these models.

### A. Reconstruction error and exponentiation

To characterize the accuracy of the various shear viscous  $\delta f$  models against fully nonlinear Bjorken evolution in 0+1D, one can use the overall RMS error  $\varepsilon(\tau)$  introduced in Sec. V. Generally we find that at early times, errors are smallest for the SR ansatz (cf. Sec. III B), whereas at late times or for large  $K_0$  the self-consistent shear corrections are the most accurate (cf. Sec. III C), which are approximated here using the power-law Grad form with exponent  $\alpha = 3/2$ . But one issue that plagues the accuracy of phase space corrections linear in  $\pi^{\mu\nu}$  is negativity. For 0+1D Bjorken evolution, the correction for the power-law Grad form is proportional to  $R_\pi(\text{sh}^2\xi - 1/2)$ , which becomes negative for  $|\xi| \gtrsim 0.66$  because in our case  $R_\pi < 0$  (cf. Fig. 1). Thus, at sufficiently high  $p_T$ , the total  $f_{eq} + \delta f$  phase space density becomes negative, which is unphysical. The  $p_T$  threshold where  $f$  turns negative drops with increasing  $|\xi|$ .

We propose to cure the negative contributions via a simple exponentiation, interpreting  $1 + \phi$  in (9) as the leading term of  $e^\phi$  near  $\phi = 0$ . This immediately renders all phase space densities positive, however, it does not ensure that the integrals for the hydrodynamic fields (27), (29), and (30) converge (e.g., for the Grad ansatz the exponent is then dominated by the quadratic terms, which are not positive definite). Therefore, we force the viscous correction in the exponent to be bounded[36] via

$$1 + \phi \rightarrow e^\phi \rightarrow e^{\tanh \phi} . \quad (45)$$

For small  $\phi$ , this still reduces to  $1 + \phi + \mathcal{O}(\phi^2)$ . Equation (45) is not the only possible solution; for example,

$$1 + \phi \rightarrow \exp\left(\beta \tanh \frac{\phi}{\beta}\right) \quad (46)$$

accomplishes the same for any  $\beta \neq 0$ , and one can even take momentum dependent  $\beta(p)$  here (with some restrictions imposed by integrability). In what follows, we refrain from fine-tuning and set  $\beta = 1$ .

Figure 2 shows the evolution of the overall RMS error as a function of normalized proper time  $\tau/\tau_0$  for initial inverse Knudsen number  $K_0 = 1$  ( $\eta/s \sim 0.2$ ). At such high viscosity, the SR model (black dashed line) has the smallest error for a wide range of times  $\tau \lesssim 13\tau_0$ . At  $\tau = \tau_0$  it is completely accurate because we chose to start the evolution from local thermal equilibrium. Moreover, at early times, errors can only accumulate quadratically with  $\tau$  because to first order in time the transport evolution starts with *free streaming*[17] (the collision term vanishes in local equilibrium), which the SR ansatz can match exactly. By  $\tau \approx 3\tau_0$ , however, the RMS error reaches 15%, and it stays roughly flat in time, decreasing only very slowly. Thus, overall, the SR ansatz is 10-15% accurate for  $K_0 = 1$ .

Figure 2 also shows results for the power-law Grad form with three exponents  $\alpha = 1$  for the RTA model (dash-dotted blue line),  $3/2$  for self-consistent shear corrections from Boltzmann transport (solid green line), and  $2$  for the Grad ansatz (dotted red line). For all three cases, the distribution was made positive via exponentiation (45). Generally, the error is largest for the RTA distribution, and smallest for the self-consistent  $\alpha = 3/2$  exponent (except at very early times  $\tau \lesssim 1.3\tau_0$  when the Grad ansatz has the largest error). At  $\tau = \tau_0$ , the power-law Grad form is completely accurate for any exponent because it admits local thermal equilibrium distributions. However, the errors quickly grow at early times, linearly with time, because the ansatz cannot describe free streaming exactly. The overall errors for

$K_0 = 1$  are quite large, reaching about 40% at  $\tau \sim 2 - 3\tau_0$  but later the accuracy improves rapidly. For  $\tau \gtrsim 13\tau_0$ , the self-consistent shear viscous  $\delta f$  has in fact smaller error than the SR ansatz, and for  $\tau \gtrsim 19\tau_0$  the Grad ansatz as well beats the SR form in accuracy.

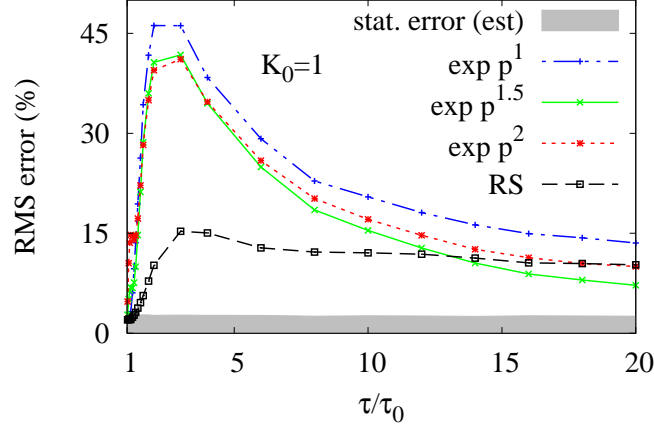


FIG. 2: Root-mean-squared phase space density reconstruction error as a function of normalized proper time  $\tau/\tau_0$  for a massless system undergoing a 0+1D Bjorken expansion with  $\eta/s \sim 0.2$  (initial inverse Knudsen number  $K_0 = 1$ ). Errors for the Strickland-Romatschke ansatz (black dashed line) are compared to those for the exponentiated power-law Grad ansatz with exponents corresponding to the RTA model ( $\alpha = 1$ , dashed-dotted blue line), self-consistent  $\delta f$  from Boltzmann transport ( $\alpha = 3/2$ , solid green line), and the Grad ansatz ( $\alpha = 2$ , dotted red line). The shaded gray band is the estimated statistical error in the analysis due to finite test particle number.

The shaded gray box in Fig. 2 indicates the inherent error due to finite statistics in the analysis. Because a stochastic Boltzmann solver is employed, counts in histogram bins have random  $\mathcal{O}(1/\sqrt{N})$  relative fluctuations. Therefore, even a perfect reconstruction model gives  $\varepsilon_{RMS} > 0$ . The inherent error for a perfect model can be estimated as

$$\varepsilon_{MIN} \approx \sqrt{\frac{1}{N_{bins}} \sum_{ij} \frac{1}{\Delta N_{tr}(p_{T,i-1} \leq p_T < p_{T,i}, \xi_{j-1} \leq \xi < \xi_j)}} , \quad (47)$$

which follows because in each bin the fluctuation in the relative error between the exact count  $\bar{N}$  and the measured count  $N$  can be estimated as

$$\left(\frac{\bar{N}}{N} - 1\right)^2 = \left(\frac{\bar{N}}{\bar{N} + \delta N} - 1\right)^2 \approx \frac{\delta N^2}{\bar{N}^2} \rightarrow \frac{1}{N} . \quad (48)$$

Note that this is a simple statistical estimate based on the actual “measured” histograms and small  $1/\sqrt{N}$  fluctuations; therefore, the shaded band is not an exact lower bound on  $\varepsilon_{RMS}$ .

The comparison changes qualitatively for smaller shear viscosities. Figure 3 shows the evolution of the overall reconstruction error for the four viscous  $\delta f$  models for initial inverse Knudsen number  $K_0 = 3.2$  ( $\eta/s \sim 0.06$ ). Compared to the  $K_0 = 1$  case, errors are reduced for all four models. For the SR ansatz (black solid line), the peak error is now only  $\approx 10\%$ , which gradually decreases to about 5% by late times  $\tau \sim 20\tau_0$ . On the other hand, there is a much bigger separation between the exponentiated power-law Grad results for the different exponents. By and large the worst choice is still the RTA ansatz ( $\alpha = 1$ , dashed-dotted blue line), followed in inaccuracy by the quadratic Grad form ( $\alpha = 2$ , dotted red line), while the most accurate reconstruction is with the self-consistent BTE corrections ( $\alpha = 3/2$ , solid green line). Unlike for  $K_0 = 1$ , for  $K_0 = 3.2$  the Grad ansatz has nearly the same accuracy as the SR form at all times  $\tau \gtrsim 2.5\tau_0$ , and at  $\tau \gtrsim 10\tau_0$  the RTA result also has similar accuracy. The best reconstruction model, however, is clearly the exponentiated power-law with the self-consistent 3/2 exponent. For  $K_0 = 3.2$ , it has comparable error to the SR ansatz at early  $\tau \sim 1.5 - 2\tau_0$ , and then progressively smaller errors than the SR ansatz and the other two power-law models at all times  $\tau \gtrsim 2\tau_0$ . In fact, by  $\tau \sim 7\tau_0$  its error becomes as small as the estimated resolution of our analysis (shaded gray band).

It is important to underscore the critical role of exponentiation in these comparisons. Without exponentiation, RMS errors for the power-law Grad form are *much* larger. For example, for  $K_0 = 1$  ( $\eta/s \sim 0.2$ ) the overall error

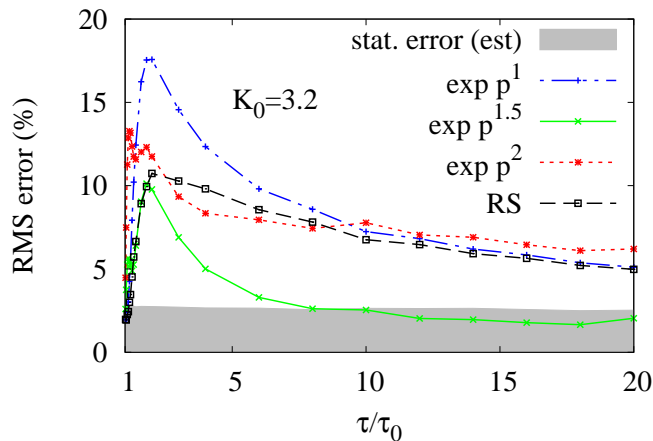


FIG. 3: The same as Fig. 2 but for about three times smaller specific shear viscosity  $\eta/s \approx 0.06$  (initial inverse Knudsen number  $K_0 = 3.2$ ).

peaks at early times near 200%, 400%, and 600% for shear viscous corrections from the RTA model, the self-consistent linearized BTE calculation, and the Grad ansatz, respectively. The same three models still give about 40%, 80% and 120% peak RMS error for  $K_0 = 3.2$  ( $\eta/s \sim 0.06$ ).

### B. Memory effect and improved $\delta f$ models based on time derivative

The transport solutions depend on both the cross section and initial conditions. Changing either results, mathematically, in a different solution. It is then natural to ask to what extent one may hope to accurately reproduce the phase space density  $f$  if only truncated information encoded in the local hydrodynamic fields is available.

To get some insight into the sensitivity of the reconstructed phase space distributions to information not captured in hydrodynamics, i.e., a memory of the transport evolution, we compare the full transport solutions at two different but hydrodynamically equivalent times. Recall the discussion in Sec. VB that the three hydrodynamic quantities available in the 0+1D Bjorken evolution considered here can be combined into an overall normalization for  $f$ , a momentum scale  $T_{eff}$ , and a dimensionless shear stress measure  $R_\pi$ . If one measures  $p_T$  relative to  $T_{eff}$ , and takes out the  $n \propto 1/\tau$  decrease in the comoving density with time, then  $R_\pi = \pi_L/p$  is the only hydrodynamic quantity that can affect the rescaled distribution function

$$\bar{f}\left(\frac{p_T}{T_{eff}}, \xi, \tau\right) \equiv \tau f(p_T, \xi, \tau). \quad (49)$$

Figure 4 shows the ratio of the rescaled transport solution at  $\tau = 2\tau_0$  to the rescaled solution at  $18\tau_0$  as a function of  $p_T/T_{eff}$  and  $\xi$ , i.e.,  $\bar{f}(p_T/T_{eff}, \xi, 2\tau_0)/\bar{f}(p_T/T_{eff}, \xi, 18\tau_0)$ , for the highest shear viscosity  $\eta/s \sim 0.2$  we studied (equivalently, the smallest inverse Knudsen number of  $K_0 = 1$ ). At both times,  $R_\pi \approx -0.168$  (cf. the stars in Fig. 1). The white region in the top right half of the plot has bins with fewer than 200 counts, therefore, the ratio is not plotted there. If the phase space densities only depended on hydrodynamic variables, the ratio would be unity. Instead, there are deviations of up to  $\sim 30\%$  in phase space. For example, at the earlier time there are 10 – 30% fewer high- $p_T$  particles at midrapidity ( $p_T \gtrsim 8T_{eff}$ ,  $|\xi| \lesssim 1$ ), and also  $\sim 10\%$  fewer particles at very low  $p_T \lesssim 0.5T_{eff}$  but high rapidity  $|\xi| \sim 1 - 2.5$ . The deficit is compensated by an excess of particles at more intermediate  $p_T \sim 2 - 6T_{eff}$  and  $|\xi| \sim 1 - 2$ . This indicates that for  $\eta/s \sim 0.2$ , it is difficult (potentially impossible) to reconstruct shear viscous phase space densities with better than roughly 5 – 10% accuracy in momentum space from the hydrodynamic fields alone at the given time.

Indeed, for systems with memory, knowledge of the current snapshot is in general insufficient to predict the future evolution. A linear theory of memory effects can be formulated using a memory kernel  $G(\tau)$  analogously to the text-book treatment of dispersion in classical electrodynamics, in which the electrical displacement  $D$  is given by the field strength  $E$  as

$$D(t) = E(t) + \int_0^\infty d\tau G(\tau)E(t - \tau). \quad (50)$$

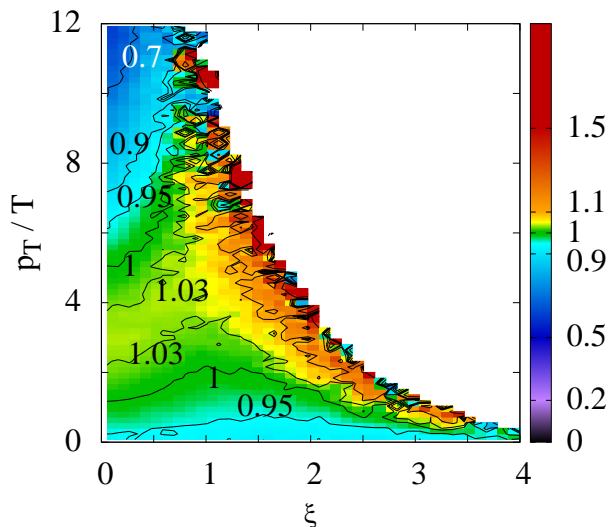


FIG. 4: Ratio of the rescaled phase space density  $\tau f(p_T/T_{eff}, \xi, \tau)$  at  $\tau = 2\tau_0$  to that at  $\tau = 18\tau_0$  as a function of normalized transverse momentum  $p_T/T_{eff}$  and rapidity  $\xi$ , calculated with MPC/Grid for massless particles with  $\eta/s \sim 0.2$  (initial inverse Knudsen number  $K_0 = 1$ ) and isotropic  $2 \rightarrow 2$  scattering. The ratio of counts in rectangular bins of size  $\Delta(p_T/T_{eff}) \times \Delta\xi \approx 0.16 \times 0.1$  is shown. Bins with fewer than 200 counts are not plotted (empty white region in the plot). Contour lines at 0.7, 0.9, 0.95, 1, and 1.03 are also shown.

This is an infinite series of time derivatives because Taylor expansion of  $E(t - \tau)$  leads to

$$D(t) = E(t) + \sum_{n=0}^{\infty} c_n \frac{d^n E(t)}{dt^n}, \quad c_n \equiv \int_0^{\infty} d\tau \frac{(-\tau)^n}{n!} G(\tau). \quad (51)$$

But if the kernel involves some short time scale  $\tau_R$ , for example,  $G(\tau) \sim e^{-\tau/\tau_R}/\tau_R$ , then  $c_n \sim \tau_R^n$  and one may truncate by only keeping the first derivative  $dE/dt$ .

To demonstrate how first time derivatives can be used to improve the modeling of viscous phase space corrections, we construct a simple model that applies the Strickland-Romatschke form during the early departure from equilibrium but switches to the exponentiated power-law Grad form with the self-consistent  $\alpha = 3/2$  exponent when the system relaxes towards local equilibrium at late times. Figure 5 shows the overall RMS error as a function of  $\tau/\tau_0$  for  $\eta/s \sim 0.2$  ( $K_0 = 1$ , thick black line), 0.1 ( $K_0 = 2$ , dashed blue line), 0.06 ( $K_0 = 3.2$ , dashed-dotted green line), and 0.03 ( $K_0 = 6.47$ , dashed-double-dotted red line). Note the log scale on the horizontal axis. For all four curves, the switch is carried out at the optimal proper time  $\tau_{switch}$  when the two models have the same RMS error (thus,  $\tau_{switch}$  depends on  $K_0$ ). To show  $\tau_{switch}$  and the higher accuracy gained by switching, the error curves for the SR ansatz are extended in the plot for  $\tau \geq \tau_{switch}$  (thin dotted lines).

Of course, a particlization model that requires the full transport solution is not very useful. In practice, one can only use information available in hydrodynamic simulations. The shear stress to pressure ratio  $R_\pi$  is insufficient because it takes the same value at both early and late times (cf. Fig. 1). However, if we also use the sign of  $dR_\pi/d\tau$ , then we can switch almost optimally with the simple rule below:

$$\begin{aligned} \text{if } R_\pi > -0.2 \text{ and } \frac{dR_\pi}{d\tau} > 0: & \text{ use the exponentiated Grad ansatz with } \alpha = 3/2, \\ \text{otherwise:} & \text{ use the Strickland - Romatschke form.} \end{aligned} \quad (52)$$

The switching times corresponding to the above simple model (filled circles in Figs. 1) and 5) close to the most optimal times, except for the largest  $K_0 = 6.47$ . In any case, the simple rules above always reduce the RMS reconstruction error compared to using the SR form at all times, and lead to markedly smaller overall error in the reconstructed phase densities at typical freezeout times  $\tau/\tau_0 \sim 5 - 20$  occurring in hydrodynamic simulations of A+A collisions at RHIC and LHC energies.

The above results advocate the development of improved viscous phase space correction models that incorporate not only the local hydrodynamic fields but their first time derivatives as well. At present, derivatives are not included in the output of hydrodynamic codes commonly used in heavy-ion physics. However, printing first derivatives of

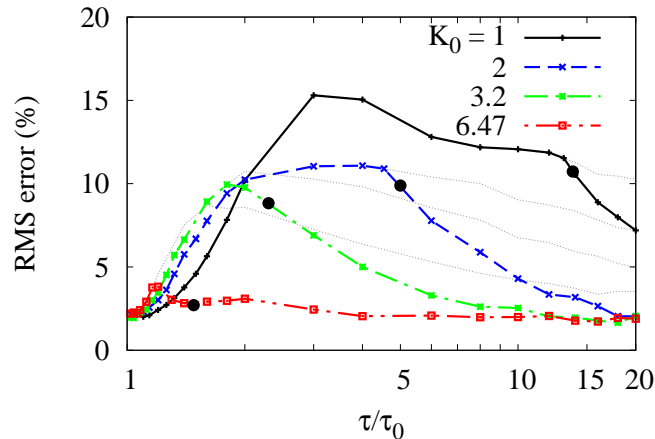


FIG. 5: Root-mean-squared reconstruction error as a function of normalized proper time  $\tau/\tau_0$  for a shear viscous  $\delta f$  model that switches between the Strickland-Romatschke ansatz and the exponentiated power-law Grad form with self-consistent  $\alpha = 3/2$  exponent. Results for initial Knudsen numbers  $K_0 = 1$  (thick black line), 2 (dotted blue line), 3.2 (dashed-dotted green line), and 6.47 (dashed-double-dotted red line) are shown. Error curves for the SR ansatz are also extended to times after the switching time (thin dotted black lines). The filled circles show the switching times for a simple model that applies the power-law Grad form whenever  $R_\pi \equiv \pi_L/p > -0.2$  and  $dR_\pi/d\tau > 0$ , while the SR ansatz otherwise.

hydrodynamic quantities should be straightforward because the hydrodynamic equations of motion are of first order in time.

## VII. CONCLUSIONS

In this work we utilized nonlinear  $2 \rightarrow 2$  kinetic theory to assess the accuracy of shear viscous phase space correction ( $\delta f$ ) models. As in Ref. [17], a massless one-component gas undergoing 0+1D Bjorken expansion with specific shear viscosity  $\eta/s \approx \text{const}$  was studied, which provides a convenient means to create a system with sustained shear. We then studied how well four different shear viscous  $\delta f$  models: the quadratic Grad form (cf. Sec. III A), the Strickland-Romatschke (SR) ansatz (cf. Sec. III B), self-consistent shear viscous corrections from linearized kinetic theory (cf. Sec. III C), and shear corrections from the relaxation time approach (RTA) (cf. Sec. III D), reproduce the full phase space distribution  $f(p_T, \xi, \tau)$  solely from the exact hydrodynamic fields corresponding to the transport solution.

In general we find that at early times the SR form is the most accurate, whereas at late times or for small  $\eta/s \sim 0.05$  the self-consistent corrections from kinetic theory perform the best. In addition, we show that the positivity of the phase space density in additive  $f = f_{\text{eq}} + \delta f$  shear correction models can be ensured via a simple exponentiation of the correction (cf. Sec. VI A), which dramatically improves the reconstruction accuracy.

Finally, we demonstrate that there is an inherent uncertainty in  $\delta f$  reconstruction because the limited information available in the hydrodynamic fields does not precisely capture the evolution history of the transport (in other words, the system has memory). We then illustrate how even more accurate viscous  $\delta f$  models can be constructed via the incorporation of the first time derivative of hydrodynamic fields, which are readily available in hydrodynamic simulations (though usually not included in the output).

Note that this work is limited to a massless one-component gas undergoing a one-dimensional Bjorken expansion. It would be very interesting to investigate in the future how well shear viscous  $\delta f$  models for mixtures, such as identified particles in a hadron gas[5], perform against full kinetic theory. Bulk viscous correction models would be similarly important to test (this requires nonzero mass). Finally, it would be important to test the improved viscous  $\delta f$  models constructed in this work in more realistic scenarios for heavy-ion reactions that include both transverse and longitudinal expansion and inhomogeneous initial geometry.

### Acknowledgments

M.D. and D.M. would like to thank the Wigner GPU Laboratory at the Wigner Research Center for Physics (Budapest, Hungary) for providing computing resources and support. D.M. also thanks the hospitality of the Brookhaven National Laboratory where parts of this work have been done. This work was supported by the US Department of Energy under grant de-sc0016524, and the Purdue Research Foundation.

- 
- [1] P. Huovinen and P. V. Ruuskanen, *Ann. Rev. Nucl. Part. Sci.* **56**, 163 (2006) [nucl-th/0605008];
- [2] C. Gale, S. Jeon and B. Schenke, *Int. J. Mod. Phys. A* **28**, 1340011 (2013) [arXiv:1301.5893 [nucl-th]].
- [3] U. Heinz and R. Snellings, *Ann. Rev. Nucl. Part. Sci.* **63**, 123 (2013) [arXiv:1301.2826 [nucl-th]].
- [4] P. Huovinen and H. Petersen, *Eur. Phys. J. A* **48**, 171 (2012) [arXiv:1206.3371 [nucl-th]].
- [5] D. Molnar and Z. Wolff, *Phys. Rev. C* **95**, no. 2, 024903 (2017) [arXiv:1404.7850 [nucl-th]].
- [6] D. Molnar, *J. Phys. G* **38**, 124173 (2011)
- [7] H. Song, S. A. Bass and U. Heinz, *Phys. Rev. C* **83**, 024912 (2011) [arXiv:1012.0555 [nucl-th]].
- [8] T. Hirano, P. Huovinen, K. Murase and Y. Nara, *Prog. Part. Nucl. Phys.* **70**, 108 (2013) [arXiv:1204.5814 [nucl-th]].
- [9] S. Ryu, S. Jeon, C. Gale, B. Schenke and C. Young, *Nucl. Phys. A904-905* **2013**, 389c (2013) [arXiv:1210.4588 [hep-ph]].
- [10] H. Grad, *Comm. Pure Appl. Math.* **2**, 331 (1949)
- [11] W. Israel and J. M. Stewart, *Annals Phys.* **118**, 341 (1979)
- [12] P. Romatschke and M. Strickland, *Phys. Rev. D* **68**, 036004 (2003) [hep-ph/0304092].
- [13] W. Florkowski, R. Ryblewski, M. Strickland and L. Tinti, *Phys. Rev. C* **89**, no. 5, 054909 (2014) [arXiv:1403.1223 [hep-ph]].
- [14] K. Dusling, G. D. Moore and D. Teaney, *Phys. Rev. C* **81**, 034907 (2010) [arXiv:0909.0754 [nucl-th]].
- [15] P. B. Arnold, G. D. Moore and L. G. Yaffe, *JHEP* **0011**, 001 (2000) [hep-ph/0010177].
- [16] W. Florkowski, E. Maksymiuk, R. Ryblewski and M. Strickland, *Phys. Rev. C* **89**, 054908 (2014)
- [17] P. Huovinen and D. Molnar, *Phys. Rev. C* **79**, 014906 (2009) [arXiv:0808.0953 [nucl-th]].
- [18] Version 2.0 of Molnar's Parton Cascade (MPC) can be downloaded from the Open Standards Codes And Routines (OSCAR) website at <http://karman.physics.purdue.edu/OSCAR>
- [19] Z. Wolff and D. Molnar, arXiv:1611.09185 [nucl-th].
- [20] S. R. de Groot, W. A. van Leeuwen, Ch. G. van Weert, *Relativistic kinetic theory - Principles and applications* (North-Holland, 1980).
- [21] L. Tinti, *Phys. Rev. C* **94**, no. 4, 044902 (2016) [arXiv:1506.07164 [hep-ph]].
- [22] M. Martinez and M. Strickland, *Nucl. Phys. A* **848**, 183 (2010) [arXiv:1007.0889 [nucl-th]].
- [23] D. Molnar and M. Gyulassy, *Phys. Rev. C* **62**, 054907 (2000) [nucl-th/0005051].
- [24] Z. Xu and C. Greiner, *Phys. Rev. C* **71**, 064901 (2005) [hep-ph/0406278].
- [25] B. Zhang, M. Gyulassy and Y. Pang, *Phys. Rev. C* **58**, 1175 (1998) [nucl-th/9801037].
- [26] F. Cooper and G. Frye, *Phys. Rev. D* **10**, 186 (1974).
- [27] GNU Scientific Library (GSL) version 1.16. Source code and documentation are available from the GNU website at <http://www.gnu.org/s/gsl>
- [28] The number current is included because, for the  $2 \rightarrow 2$  transport considered here, it is conserved.
- [29] We consider Boltzmann statistics throughout, however, extension to the Fermi/Bose case is straightforward.
- [30] The decomposition depends on the choice of the fluid flow velocity field  $u^\mu(x)$  that enters in  $f_{\text{eq}}$  (cf. (2)). Here we follow the Landau prescription that a local observer at  $x$  comoving with the fluid should find no energy flow at  $x$ .
- [31] For the massless gas considered later in this work, bulk pressure vanishes identically because the energy-momentum tensor (1) is traceless.
- [32] By longitudinal boost invariance we mean that the state of the system at each point in spacetime with  $t > 0$ ,  $z \neq 0$  can be obtained from the state on the  $z = 0$  sheet via Lorentz boost along the  $z$  direction.
- [33] The momentum distribution of particles crossing a three-dimensional hypersurface at spacetime coordinate  $x$  is [26]

$$E \frac{dN}{d^3p} = p^\mu d\sigma_\mu(x) f(x, \mathbf{p}) ,$$

where  $d\sigma^\mu$  is the Minkowski normal to the hypersurface at  $x$ . For  $\tau = \text{const}$  hypersurfaces,  $p^\mu d\sigma_\mu = m_T \text{ch}\xi \tau d^2x_T d\eta$ , where  $m_T \equiv \sqrt{p_T^2 + m^2}$  and  $\mathbf{x}_T$  are the transverse mass and position. Substitution of  $d^3p/E \equiv d^2p_T dy$  with a switch to polar coordinates in the transverse plane leads to (31) for massless particles.

- [34] For a massless gas in chemical equilibrium,  $s = 4n$ . Out of chemical equilibrium, the factor of 4 shifts to  $4 - \ln(n/n_{\text{eq}})$ , which is usually a modest correction only.
- [35] If in doubt, recast (32), (33) and (34) in terms of dimensionless  $q \equiv p_T/T$  for the power-law Grad form to find

$$e \propto NT^4 , \quad \pi_L \propto NT^4 , \quad n \propto NT^3 ,$$

where the dimensionless proportionality constants only depend on  $R_\pi$ . Analogous results follow for the SR ansatz but with  $\Lambda$  instead of  $T$ , and  $a$  instead of  $R_\pi$ .

[36] Alternatively, one could divide  $\phi$  in the exponent by a momentum dependent function that at large momenta fixes the asymptotic behavior whereas at low momenta stays approximately constant.